

DTIC FILE COPY

4

RADC-TR-89-216
Final Technical Report
October 1989



AD-A217 079

TWO-DIMENSIONAL SIMULATIONS OF A CHARGE-NEUTRAL PLASMA BEAM INJECTED INTO A TRANSVERSE MAGNETIC FIELD

Institute of Geophysics & Planetary Physics (UCLA)

W.A. Livesey and P.L. Pritchett

DTIC
ELECTE
JAN 19 1990
3E D

APPROVED FOR PUBLIC RELEASE; DISTRIBUTION UNLIMITED.

ROME AIR DEVELOPMENT CENTER
Air Force Systems Command
Griffiss Air Force Base, NY 13441-5700

90 01 18 077

This report has been reviewed by the RADC Public Affairs Division (PA) and is releasable to the National Technical Information Service (NTIS). At NTIS it will be releasable to the general public, including foreign nations.

RADC-TR-89-216 has been reviewed and is approved for publication.

APPROVED:



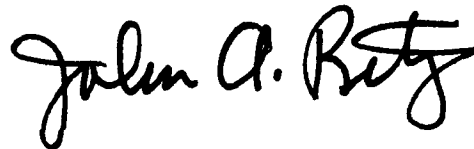
DELIA E. DONATELLI
Project Engineer

APPROVED:



JOHN K. SCHINDLER
Director of Electromagnetics

FOR THE COMMANDER:



JOHN A. RITZ
Directorate of Plans & Programs

If your address has changed or if you wish to be removed from the RADC mailing list, or if the addressee is no longer employed by your organization, please notify RADC (EECP) Hanscom AFB MA 01731-5000. This will assist us in maintaining a current mailing list.

Do not return copies of this report unless contractual obligations or notices on a specific document require that it be returned.

UNCLASSIFIED

SECURITY CLASSIFICATION OF THIS PAGE

REPORT DOCUMENTATION PAGE				Form Approved OMB No 0704-0188	
1a. REPORT SECURITY CLASSIFICATION UNCLASSIFIED			1b. RESTRICTIVE MARKINGS N/A		
2a. SECURITY CLASSIFICATION AUTHORITY N/A			3. DISTRIBUTION/AVAILABILITY OF REPORT Approved for public release; distribution unlimited.		
2b. DECLASSIFICATION/DOWNGRADING SCHEDULE N/A			5. MONITORING ORGANIZATION REPORT NUMBER(S) RADC-TR-89-216		
4. PERFORMING ORGANIZATION REPORT NUMBER(S) N/A			7a. NAME OF MONITORING ORGANIZATION Rome Air Development Center (EECP)		
6a. NAME OF PERFORMING ORGANIZATION Institute of Geophysics & Planetary Physics (UCLA)		6b. OFFICE SYMBOL (If applicable)		7b. ADDRESS (City, State, and ZIP Code) Hanscom AFB MA 01731-5000	
6c. ADDRESS (City, State, and ZIP Code) 405 Hilgard Avenue Los Angeles CA 90024-1567		8a. NAME OF FUNDING/SPONSORING ORGANIZATION Rome Air Development Center		9. PROCUREMENT INSTRUMENT IDENTIFICATION NUMBER F30602-81-C-0206	
8b. OFFICE SYMBOL (If applicable) EECP		10. SOURCE OF FUNDING NUMBERS			
8c. ADDRESS (City, State, and ZIP Code) Hanscom AFB MA 01731-5000		PROGRAM ELEMENT NO 61102F	PROJECT NO 2305	TASK NO J2	WORK UNIT ACCESSION NO P1
11. TITLE (Include Security Classification) TWO-DIMENSIONAL SIMULATIONS OF A CHARGE-NEUTRAL PLASMA BEAM INJECTED INTO A TRANSVERSE MAGNETIC FIELD					
12. PERSONAL AUTHOR(S) W. A. Livesey, P. L. Pritchett					
13a. TYPE OF REPORT Final		13b. TIME COVERED FROM Mar 87 TO Dec 87		14. DATE OF REPORT (Year, Month, Day) October 1989	
15. PAGE COUNT 36					
16. SUPPLEMENTARY NOTATION N/A					
17. COSATI CODES			18. SUBJECT TERMS (Continue on reverse if necessary and identify by block number)		
FIELD	GROUP	SUB-GROUP	Plasma Simulation Low-Frequency Communications		
17	02		Spacecraft Charging		
20	14		ULF Antenna		
19. ABSTRACT (Continue on reverse if necessary and identify by block number) It has been suggested that a charge-neutral beam consisting of ions and electrons may serve as an alternate to the plasma contractor for collecting electrons from the ionosphere. The collecting area of the beam would be determined by the distance it can penetrate the local magnetic field. A charge-neutral beam can transverse a magnetic field by virtue of collective effects for the proper parameter regime. This phenomenon is studied using a two-dimensional (three-velocity) electrostatic code. A polarization electric field forms across the beam as it penetrates the magnetic field. In vacuum the beam penetrates $4.5\rho_i$ into the field, ρ_i a gyroradius of a beam ion traveling at injection velocity. Loss of ions from the polarization layer produces a net electron current in the beam. The beam curves slightly due to the resulting $j \times B$ force. Injection into a tenuous plasma with a plasma-to-beam density ratio of 1/100 shortens the penetration length to $2.7\rho_i$. The plasma partially shields the polarization field of the beam. Consequently, more beam ions are lost. The net beam current is enhanced resulting in a more pronounced curvature. (Continued on Reverse)					
20. DISTRIBUTION/AVAILABILITY OF ABSTRACT <input checked="" type="checkbox"/> UNCLASSIFIED/UNLIMITED <input type="checkbox"/> SAME AS RPT. <input type="checkbox"/> DTIC USERS			21. ABSTRACT SECURITY CLASSIFICATION UNCLASSIFIED		
22a. NAME OF RESPONSIBLE INDIVIDUAL Delia E. Donatelli			22b. TELEPHONE (Include Area Code) (617) 377-2986		22c. OFFICE SYMBOL RADC (EECP)

DD Form 1473, JUN 86

Previous editions are obsolete.

SECURITY CLASSIFICATION OF THIS PAGE
UNCLASSIFIED

UNCLASSIFIED

Block 19 Continued:

Injection into a marginally dense plasma with a density ratio of 1/10 results in a pronounced deflection of the beam.

ABC _____ OF _____
 DE _____ ☒ _____
 F _____ ☐ _____
 G _____ ☐ _____
 H _____
 I _____
 J _____ on _____
 K _____
 L _____
 M _____
 N _____
 O _____
 P _____
 Q _____
 R _____
 S _____
 T _____
 U _____
 V _____
 W _____
 X _____
 Y _____
 Z _____
 AA _____
 AB _____
 AC _____
 AD _____
 AE _____
 AF _____
 AG _____
 AH _____
 AI _____
 AJ _____
 AK _____
 AL _____
 AM _____
 AN _____
 AO _____
 AP _____
 AQ _____
 AR _____
 AS _____
 AT _____
 AU _____
 AV _____
 AW _____
 AX _____
 AY _____
 AZ _____
 BA _____
 BB _____
 BC _____
 BD _____
 BE _____
 BF _____
 BG _____
 BH _____
 BI _____
 BJ _____
 BK _____
 BL _____
 BM _____
 BN _____
 BO _____
 BP _____
 BQ _____
 BR _____
 BS _____
 BT _____
 BU _____
 BV _____
 BW _____
 BX _____
 BY _____
 BZ _____
 CA _____
 CB _____
 CC _____
 CD _____
 CE _____
 CF _____
 CG _____
 CH _____
 CI _____
 CJ _____
 CK _____
 CL _____
 CM _____
 CN _____
 CO _____
 CP _____
 CQ _____
 CR _____
 CS _____
 CT _____
 CU _____
 CV _____
 CW _____
 CX _____
 CY _____
 CZ _____
 DA _____
 DB _____
 DC _____
 DD _____
 DE _____
 DF _____
 DG _____
 DH _____
 DI _____
 DJ _____
 DK _____
 DL _____
 DM _____
 DN _____
 DO _____
 DP _____
 DQ _____
 DR _____
 DS _____
 DT _____
 DU _____
 DV _____
 DW _____
 DX _____
 DY _____
 DZ _____
 EA _____
 EB _____
 EC _____
 ED _____
 EE _____
 EF _____
 EG _____
 EH _____
 EI _____
 EJ _____
 EK _____
 EL _____
 EM _____
 EN _____
 EO _____
 EP _____
 EQ _____
 ER _____
 ES _____
 ET _____
 EU _____
 EV _____
 EW _____
 EX _____
 EY _____
 EZ _____
 FA _____
 FB _____
 FC _____
 FD _____
 FE _____
 FF _____
 FG _____
 FH _____
 FI _____
 FJ _____
 FK _____
 FL _____
 FM _____
 FN _____
 FO _____
 FP _____
 FQ _____
 FR _____
 FS _____
 FT _____
 FU _____
 FV _____
 FW _____
 FX _____
 FY _____
 FZ _____
 GA _____
 GB _____
 GC _____
 GD _____
 GE _____
 GF _____
 GG _____
 GH _____
 GI _____
 GJ _____
 GK _____
 GL _____
 GM _____
 GN _____
 GO _____
 GP _____
 GQ _____
 GR _____
 GS _____
 GT _____
 GU _____
 GV _____
 GW _____
 GX _____
 GY _____
 GZ _____
 HA _____
 HB _____
 HC _____
 HD _____
 HE _____
 HF _____
 HG _____
 HH _____
 HI _____
 HJ _____
 HK _____
 HL _____
 HM _____
 HN _____
 HO _____
 HP _____
 HQ _____
 HR _____
 HS _____
 HT _____
 HU _____
 HV _____
 HW _____
 HX _____
 HY _____
 HZ _____
 IA _____
 IB _____
 IC _____
 ID _____
 IE _____
 IF _____
 IG _____
 IH _____
 II _____
 IJ _____
 IK _____
 IL _____
 IM _____
 IN _____
 IO _____
 IP _____
 IQ _____
 IR _____
 IS _____
 IT _____
 IU _____
 IV _____
 IW _____
 IX _____
 IY _____
 IZ _____
 JA _____
 JB _____
 JC _____
 JD _____
 JE _____
 JF _____
 JG _____
 JH _____
 JI _____
 JJ _____
 JK _____
 JL _____
 JM _____
 JN _____
 JO _____
 JP _____
 JQ _____
 JR _____
 JS _____
 JT _____
 JU _____
 JV _____
 JW _____
 JX _____
 JY _____
 JZ _____
 KA _____
 KB _____
 KC _____
 KD _____
 KE _____
 KF _____
 KG _____
 KH _____
 KI _____
 KJ _____
 KK _____
 KL _____
 KM _____
 KN _____
 KO _____
 KP _____
 KQ _____
 KR _____
 KS _____
 KT _____
 KU _____
 KV _____
 KW _____
 KX _____
 KY _____
 KZ _____
 LA _____
 LB _____
 LC _____
 LD _____
 LE _____
 LF _____
 LG _____
 LH _____
 LI _____
 LJ _____
 LK _____
 LL _____
 LM _____
 LN _____
 LO _____
 LP _____
 LQ _____
 LR _____
 LS _____
 LT _____
 LU _____
 LV _____
 LW _____
 LX _____
 LY _____
 LZ _____
 MA _____
 MB _____
 MC _____
 MD _____
 ME _____
 MF _____
 MG _____
 MH _____
 MI _____
 MJ _____
 MK _____
 ML _____
 MM _____
 MN _____
 MO _____
 MP _____
 MQ _____
 MR _____
 MS _____
 MT _____
 MU _____
 MV _____
 MW _____
 MX _____
 MY _____
 MZ _____
 NA _____
 NB _____
 NC _____
 ND _____
 NE _____
 NF _____
 NG _____
 NH _____
 NI _____
 NJ _____
 NK _____
 NL _____
 NM _____
 NN _____
 NO _____
 NP _____
 NQ _____
 NR _____
 NS _____
 NT _____
 NU _____
 NV _____
 NW _____
 NX _____
 NY _____
 NZ _____
 OA _____
 OB _____
 OC _____
 OD _____
 OE _____
 OF _____
 OG _____
 OH _____
 OI _____
 OJ _____
 OK _____
 OL _____
 OM _____
 ON _____
 OO _____
 OP _____
 OQ _____
 OR _____
 OS _____
 OT _____
 OU _____
 OV _____
 OW _____
 OX _____
 OY _____
 OZ _____
 PA _____
 PB _____
 PC _____
 PD _____
 PE _____
 PF _____
 PG _____
 PH _____
 PI _____
 PJ _____
 PK _____
 PL _____
 PM _____
 PN _____
 PO _____
 PP _____
 PQ _____
 PR _____
 PS _____
 PT _____
 PU _____
 PV _____
 PW _____
 PX _____
 PY _____
 PZ _____
 QA _____
 QB _____
 QC _____
 QD _____
 QE _____
 QF _____
 QG _____
 QH _____
 QI _____
 QJ _____
 QK _____
 QL _____
 QM _____
 QN _____
 QO _____
 QP _____
 QQ _____
 QR _____
 QS _____
 QT _____
 QU _____
 QV _____
 QW _____
 QX _____
 QY _____
 QZ _____
 RA _____
 RB _____
 RC _____
 RD _____
 RE _____
 RF _____
 RG _____
 RH _____
 RI _____
 RJ _____
 RK _____
 RL _____
 RM _____
 RN _____
 RO _____
 RP _____
 RQ _____
 RR _____
 RS _____
 RT _____
 RU _____
 RV _____
 RW _____
 RX _____
 RY _____
 RZ _____
 SA _____
 SB _____
 SC _____
 SD _____
 SE _____
 SF _____
 SG _____
 SH _____
 SI _____
 SJ _____
 SK _____
 SL _____
 SM _____
 SN _____
 SO _____
 SP _____
 SQ _____
 SR _____
 SS _____
 ST _____
 SU _____
 SV _____
 SW _____
 SX _____
 SY _____
 SZ _____
 TA _____
 TB _____
 TC _____
 TD _____
 TE _____
 TF _____
 TG _____
 TH _____
 TI _____
 TJ _____
 TK _____
 TL _____
 TM _____
 TN _____
 TO _____
 TP _____
 TQ _____
 TR _____
 TS _____
 TT _____
 TU _____
 TV _____
 TW _____
 TX _____
 TY _____
 TZ _____
 UA _____
 UB _____
 UC _____
 UD _____
 UE _____
 UF _____
 UG _____
 UH _____
 UI _____
 UJ _____
 UK _____
 UL _____
 UM _____
 UN _____
 UO _____
 UP _____
 UQ _____
 UR _____
 US _____
 UT _____
 UU _____
 UV _____
 UW _____
 UX _____
 UY _____
 UZ _____
 VA _____
 VB _____<

A-1



UNCLASSIFIED

CONTENTS

		<u>Page</u>
Paragraph 1	INTRODUCTION	1
2	SIMULATION PARAMETERS	5
3	INJECTION INTO VACUUM	7
3.1	Nonpropagating Beam	7
3.2	Propagating Beam	7
3.2.1	Beam densities and potential contour plots	7
3.2.2	Beam density and current plots	13
4	INJECTION INTO A LOW-DENSITY PLASMA	15
4.1	Beam Properties as a Function of Relative Density . . .	15
4.1.1	Beam density and potential contour plots for ambient plasma	15
4.1.2	Potential contour plots	20
4.2	Response of the Ambient Plasma	19
5	SUMMARY AND CONCLUSIONS	24

FIGURES

		<u>Page</u>
Figure 1.	Schematic diagram of injected beam. (a) Particles gyrate due to Lorentz force. (b) Space-charge layers form and establish polarization field	2
2.	Example of nonpropagating beam. Dotted lines are electron contours. Solid lines are ion contours	8
3.	Example of beam propagating in vacuum. Minimum density contour is 10% of injection value. Beam curves upward slightly	9
4.	Time-sequence of beam propagating in vacuum. Species are superimposed. Dotted lines are electron contours. Solid lines are ion contours. Minimum density contour is 1% of injection value. Dashed line represents a gyrating ion trajectory. Ions are lost from lower space-charge layer	10

FIGURES

Page

Figure	5.	Time-sequence of potential lines for the vacuum propagation case. Potential lines in beam separate as ions are lost from space-charge layer	12
	6.	Beam current plot for vacuum case. Ion density contour and current plots are shown separately. Current in right half and lower edge of beam appears to produce $\vec{j} \times \vec{B}$ force to curve beam upward	14
	7.	Example of beam propagating in tenuous plasma ($n_p/n_b = 1/100$). Minimum density contour is 10% of injection value. Beam curvature is more pronounced than the vacuum case	16
	8.	Example of beam propagating in marginally dense plasma ($n_p/n_b = 1/10$). Minimum density contour is 10% of injection value. Beam curvature is very abrupt	17
	9.	Comparison of density profiles for beams which have propagated for $t = 320\omega_{be}^{-1}$. Cross-sections are taken at $x = 16l\Delta$. (a) Vacuum. (b) Tenuous plasma. (c) Marginally dense plasma	18
	10.	Beam current plot for tenuous plasma case ($n_p/n_b = 1/100$). Ion density contour and current plots are shown separately. Current in lower edge appears to produce $\vec{j} \times \vec{B}$ force to curve beam upward	20
	11.	Potential plots of beams which have propagated for $t = 320\omega_{be}^{-1}$. (a) Vacuum. (b) Tenuous plasma. (c) Marginally dense plasma	21
	12.	Ambient current plot for tenuous plasma case ($n_p/n_b = 1/100$). Ion density contour is superimposed. (a) Ambient ion current. (b) Ambient electron current	23

1. INTRODUCTION

The injection and propagation of a charge-neutral beam across a magnetic field has been the subject of several theoretical and experimental studies.¹⁻⁹ Such beams have been considered for use in tokamak heating¹⁰ and driving currents in a magnetically confined plasma.¹¹ Charge-neutral beams have also begun to supplement electron beams as a means to actively probe the ionosphere.¹²⁻¹⁷

Our interest in the problem of injecting a plasma beam across a magnetic field stems from the need to control spacecraft charging during electron beam experiments. A spacecraft may not be able to collect sufficient numbers of electrons from the ionosphere to compensate for those emitted in the beam. A plasma beam injected transverse to the ambient magnetic field might serve to collect electrons traveling along the field lines during electron beam experiments. The collecting area of the plasma beam would depend on how far it could penetrate the field. This idea is closely allied to that of the plasma contactor currently in use. There is also the possibility of using a charge-neutral beam as an ULF antenna provided the beam can be made long enough.

A beam injected into a transverse magnetic field may be categorized by the ratio of its radius R to that of an ion gyroradius ρ_i .^{4,5} The case of $R/\rho_i \gg 1$ is termed a small-gyroradius beam while that of $R/\rho_i \lesssim 1$ is termed a large-gyroradius beam. The mechanism by which the beam penetrates the magnetic field also serves to characterize it. The completely diamagnetic plasma with a kinetic $\beta \gg 1$ represents one extreme. For this case the plasma expels the magnetic field from its interior and propagates ballistically.¹⁸⁻²⁰ The other extreme is the beam which is completely nondiamagnetic as it penetrates the transverse field. In the nondiamagnetic case the beam may propagate by means of electric polarization.^{18,21,22} The electric polarization of the beam arises from space-charge separation layers forming due to the Lorentz force. The work to be presented here is restricted to the nondiamagnetic regime for the large-gyroradius case.

The beam geometry used is shown in Figure 1. The beam is injected in the \hat{x} direction with velocity v_b transverse to a uniform magnetic field B_z . The beam has a finite height h in the \hat{y} direction and is infinite along \hat{z} . When the beam crosses the magnetic field the electrons and ions in the head of the beam initially gyrate in opposite directions. The ensuing current J_y creates space-charge boundary layers on either side of the beam. The accumulation of charge

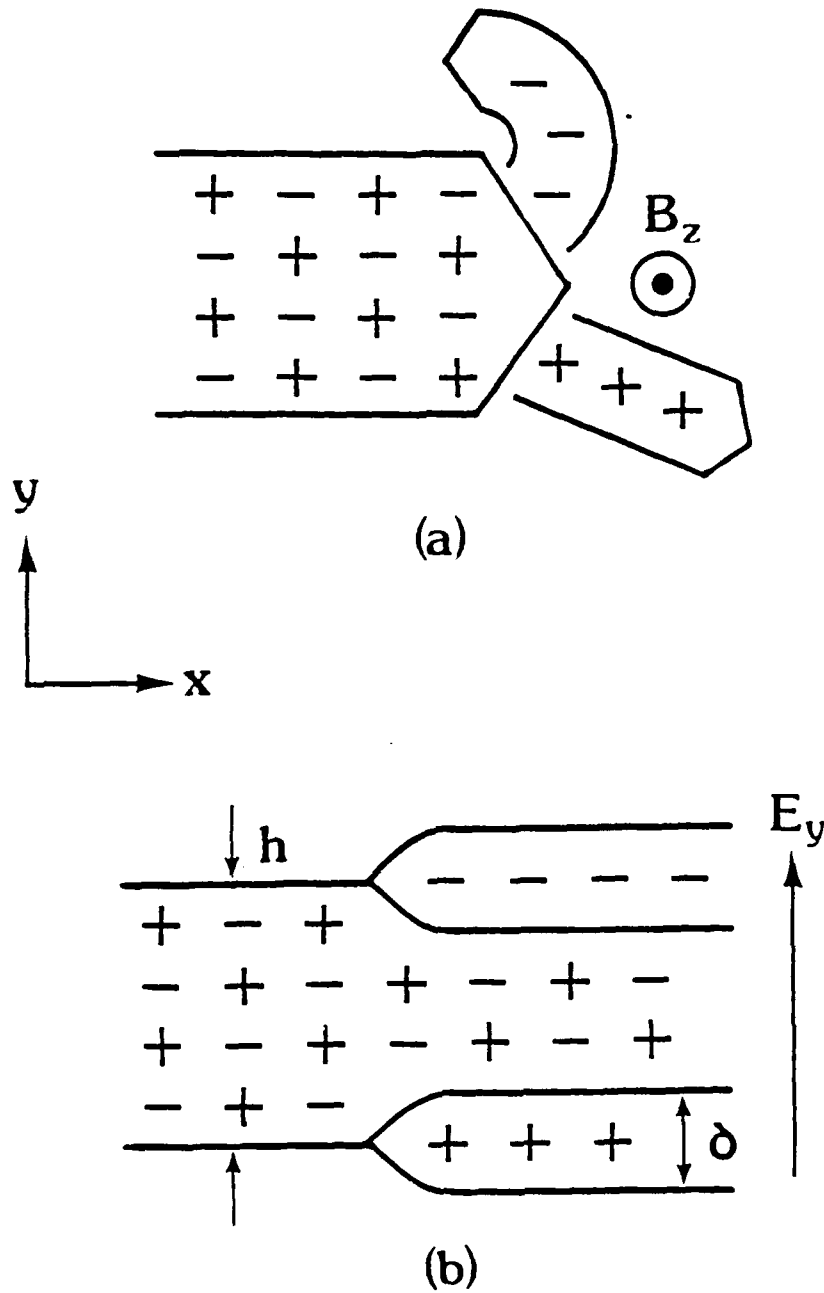


Figure 1. Schematic diagram of injected beam. (a) Particles gyrate due to Lorentz force. (b) Space-charge layers form and establish polarization field.

on the boundaries gives rise to a transverse electric field \vec{E}_y . This polarization field will result in the beam particles acquiring an $\vec{E} \times \vec{B}$ drift across the magnetic field.

A theory for the steady-state polarization drift has been determined by Schmidt.²² The first requirement is that the beam possess a kinetic energy density much greater than the polarization field energy density. The additional requirement that the beam $\vec{E} \times \vec{B}$ drift with approximately the initial injection velocity yields

$$\epsilon - 1 \geq \frac{\omega_{pi}^2}{\Omega_i^2} \gg 1, \quad (1)$$

where ϵ is the dielectric constant of the beam plasma, ω_{pi} is the ion plasma frequency, and Ω_i is the ion gyrofrequency. It has been further shown⁵ that a condition for charge neutrality is

$$\epsilon \gg \left(\frac{m_{bi}}{m_e} \right)^{1/2}, \quad (2)$$

where m_{bi}/m_e is the beam ion to electron mass ratio.

A second necessary condition for the polarization drift model to work is that the space-charge boundary layer be significantly smaller than the beam height. This is expressed as

$$\delta = \rho_i / (\epsilon - 1) \ll h. \quad (3)$$

This represents the lower limit of the beam height. An upper limit is established by requiring that the maximum potential difference across the beam cannot exceed the initial kinetic energy which the ions are accelerated to.²³ Thus, $eE_y h < Mv_h^2/2$, and may be written as

$$h < \rho_i / 2. \quad (4)$$

A charge-neutral beam is expected to propagate across a transverse field if these conditions are satisfied. The time-averaged drift velocity of the beam⁵ is given by

$$v_x = v_b (1 - 1/\epsilon). \quad (5)$$

The drift velocity is very nearly the injection velocity for $\epsilon \gg 1$.

In section 2 the parameters used in the simulations are described. Beam injection into a vacuum is presented in section 3. For vacuum injection two cases are considered. The parameters of the first case do not satisfy the requirements for the polarization drift model and the beam separates into its charged components. For the second case the polarization requirements are satisfied and the beam does propagate. However, the beam curves slightly in the direction of initial electron gyration. Section 4 deals with injection into a tenuous magnetized plasma where the mass of the plasma ions is equal to the mass of the beam ions. With an ambient plasma present of density $n_p/n_b = 1/100$, the curvature of the beam is noticeably increased. For the case of $n_p/n_b = 1/10$, the beam curves sharply in the direction of electron gyration and then in the opposite direction. Results are summarized in section 5.

2. SIMULATION PARAMETERS

The injection of the beam and the response of the beam and ambient plasma are investigated with two-dimensional (three-velocity) electrostatic full-particle simulations. The simulation model treats the beam source, the beam itself, and any ambient plasma as an isolated system; periodic boundary conditions are not employed. The simulation code is the same as used by Pritchett and Winglee²⁴ for electron beam studies and Winglee and Pritchett²⁵ for charge-neutral beam studies. In this study, as in the study by Winglee and Pritchett²⁵, the beam is charge-neutral rather than consisting solely of electrons. The mass of the beam ions m_{bi} is 100 times the electron mass m_e . When ambient plasma is present the mass of the beam ions m_{bi} is equal to the mass of the ambient ions m_{pi} . The magnetic field is directed along the z axis (out of the simulation plane) and is constant throughout the volume of the simulation box. In most of the examples presented the magnetic field strength is such that the ratio of electron cyclotron frequency Ω_e to the beam-electron plasma frequency ω_{be} is $\Omega_e/\omega_{be} = 1/4$. The unit of length in the simulations is the grid spacing Δ and the unit of time is the inverse beam-electron plasma frequency ω_{be}^{-1} , where $\omega_{be} = (n_{b0}e^2/\epsilon_0 m_{be})^{1/2}$, and n_{b0} is the beam density at injection. The initial velocity v_b is typically $0.5\Delta\omega_{be}$. An ion gyroradius is typically 200Δ . For a 400 eV Argon beam injected across a 0.25 gauss field Δ is about 3.6 m. The system dimensions are $L_x = 512\Delta$ and $L_y = 64\Delta$ or 128Δ . The time step in the simulation is typically $\Delta t = 0.1/\omega_{be}$. The largest system of particles consists of 224,000 particles and the smallest consists of 138,500. The beam at injection has a height $h = 10\Delta$ perpendicular to the magnetic field. For $\Omega_e/\omega_{be} = 1/4$ the beam height is 20 times the beam electron gyroradius and 1/20 of the beam ion gyroradius for the parameters considered in this work. The thermal electron velocity is typically $0.5\Delta\omega_{be}$ and the thermal ion velocity is typically $0.05\Delta\omega_{be}$.

The beam is injected from the center of the right-hand side of an idealized spacecraft. A particle which encounters the boundary of the spacecraft is removed from the system and its charge uniformly distributed on the surface of the spacecraft. The beam is taken to be charge-neutral so the injection process leaves no net charge on the spacecraft. However, spacecraft charging can occur if particles are accelerated onto the spacecraft by fields produced by space-charge effects. The spacecraft has the dimensions of $6\Delta \times 12\Delta$ to allow

for the collection of such a charge. The center of the spacecraft is located at $(0.11 L_x, 0.50 L_y)$.

Ambient plasma is reflected from the boundaries of the simulation box while beam particles are allowed to escape. This feature of the simulation model remains valid provided the plasma is basically undisturbed near the boundary. A loss of 4% of the beam particles is considered excessive and the simulations are assumed invalid beyond that point.

3. INJECTION INTO VACUUM

In this section we examine the behavior of a charge-neutral beam injected transverse to a constant vacuum magnetic field. Two cases are considered. The first has parameters which violate some of the polarization drift model criteria. As such, it would not be expected to propagate through the magnetic field by virtue of collective effects. The second case is typical of the simulation parameters presented in section 2 and does exhibit the expected polarization drift.

3.1 Nonpropagating Beam. For the nonpropagating example the injection velocity $v_b = 10\Delta\omega_{be}$ and the magnetic field is $B_e/\omega_{be} = 1.0$. The beam height is $h = 10\Delta$. The beam ion mass to electron mass ratio is $m_{bi}/m_e = 100$. The ion gyroradius is then $\rho_i = 1000\Delta$. The dielectric constant of the beam is $\epsilon = 100$. This marginally satisfies the requirement $\epsilon \gg (m_{bi}/m_e)^{1/2}$. The space-charge boundary layer thickness is $\delta = 10\Delta$ and is equal to the beam height, a clear violation of the polarization model criteria.

Figure 2 shows contour plots of charge density for this case shortly after injection is initiated. The dotted contours indicate regions where electron charge density dominates while the solid contours indicate regions dominated by positive charge. The spacecraft is negatively charged and represented by the rectangular contours behind the injection plane at $x = 60\Delta$. Upon injection the initially charge-neutral beam separates into charged beams, an ion beam and an electron beam, which gyrate in the magnetic field. The beam polarization drift is not observed in this case.

3.2 Propagating Beam. The example of the propagating beam is typical of the simulation parameters used throughout the rest of this study. The dielectric constant for this case is $\epsilon = 1600$ which easily satisfies the requirement $\epsilon \gg (m_{bi}/m_e)^{1/2} = 10$. The space-charge boundary layer thickness is $\delta = 0.125\Delta$. The beam height is $h = 10\Delta$; consequently the requirement that $\delta \ll h$ is satisfied.

3.2.1 Beam density and potential contour plots. Figure 3 shows separate beam density contour plots for the electrons and ions. The minimum contour value in these plots is 10% of the injection density. During a period of

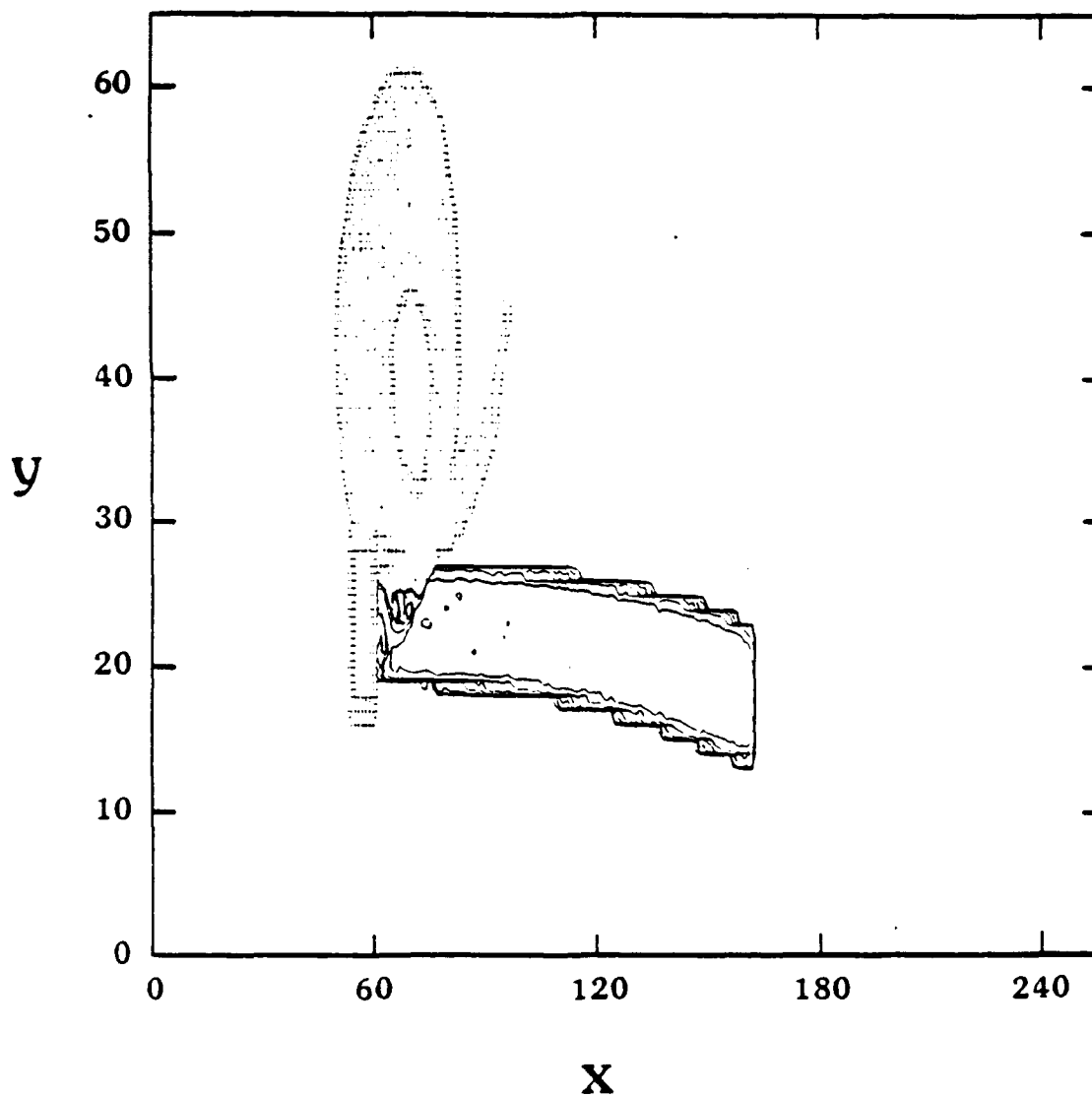


Figure 2. Example of nonpropagating beam. Dotted lines are electron contours. Solid lines are ion contours.

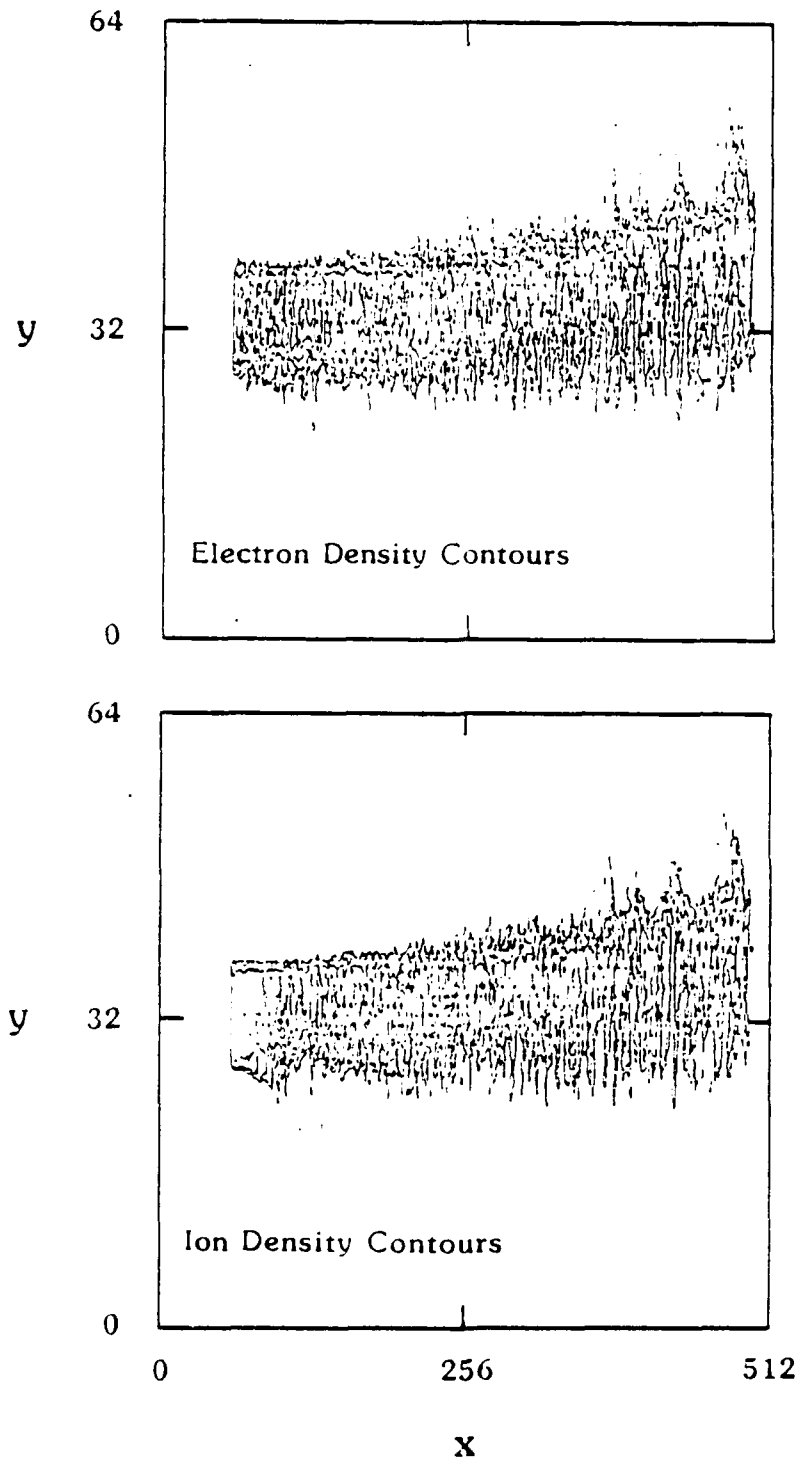


Figure 3. Example of beam propagating in vacuum. Minimum density contour is 10% of injection value. Beam curves upward slightly.

$880\omega_{be}^{-1}$ the head of the beam travels from the initial injection plane at $x = 60\Delta$ to approximately $x = 500\Delta$. This yields an average propagation velocity of $v_x = 0.54\omega_{be}$, which is the initial injection velocity, an expected result. Close examination of the beam contours reveals a slight curvature of the beam path of both ions and electrons. The beam is deflected in the \hat{y} direction, which is opposite to that in which the beam ions would initially gyrate.

At the end of the run the head of the beam has expanded to a height of approximately $h = 15\Delta$ and traveled $x = 2.2\rho_i$. Both spreading and particle loss from the space-charge layers degrade the density of the charge-neutral region within the beam. The density of the charge-neutral region has been estimated at $x = 161\Delta$, 261Δ , and 361Δ and shows a noticeable decrease. Linear extrapolation of these density values suggests the beam will degrade to 10% of the injection value after traveling $4.5\rho_i$.

Figure 4 shows contour plots of the charge density with the minimum contour line equal to 1% of the injection density. As before, the dotted lines indicate regions of negative charge density and the solid lines indicate positive charge density regions. The beam is shown evolving over a period of $160\omega_{be}^{-1}$. The most striking feature of this plot is the asymmetric loss of ions from the lower, or positively charged, side of the beam. Ions at the outer surface of the positive space-charge boundary layer are partially shielded from the electric polarization field and can eventually gyrate away from the beam. The dashed line on the lower side of the beam represents a gyro-orbit of an ion moving at the injection velocity. An additional noteworthy feature is the conspicuous bulge of electrons above the head of the beam.

Electric potential contour plots to accompany Figure 4 are shown in Figure 5. As the beam transverses the magnetic field a potential distribution forms which has a gradient perpendicular to both the magnetic field and the direction of beam injection. The dotted lines indicate regions of negative potential and the solid lines indicate regions of positive potential. From the first two panels of the plot it is evident that within the beam region the electric field is primarily in the \hat{y} direction. The gradient in the potential contours at the front, or head, of the beam indicate a rearward pointing electric field above the beam and a forward pointing field below the beam. The electrons on the outer edge of the beam head are extruded outward from the beam by virtue of the resulting $\vec{E} \times \vec{B}$ drift and produces the electron bulge.

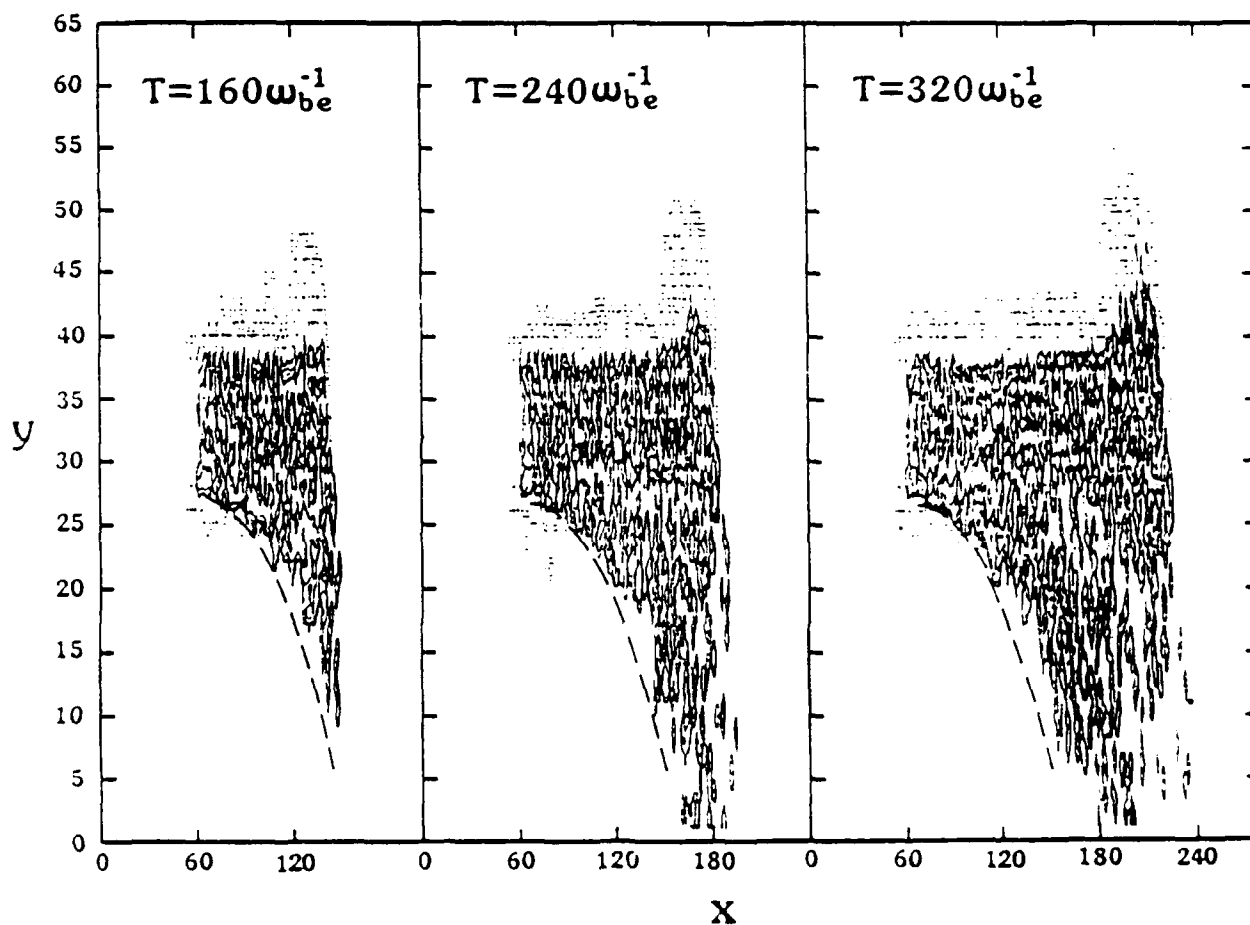


Figure 4. Time-sequence of beam propagating in vacuum. Species are superimposed. Dotted lines are electron contours. Solid lines are ion contours. Minimum density contour is 1% of injection value. Dashed line represents a gyrating ion trajectory. Ions are lost from lower space-charge layer.

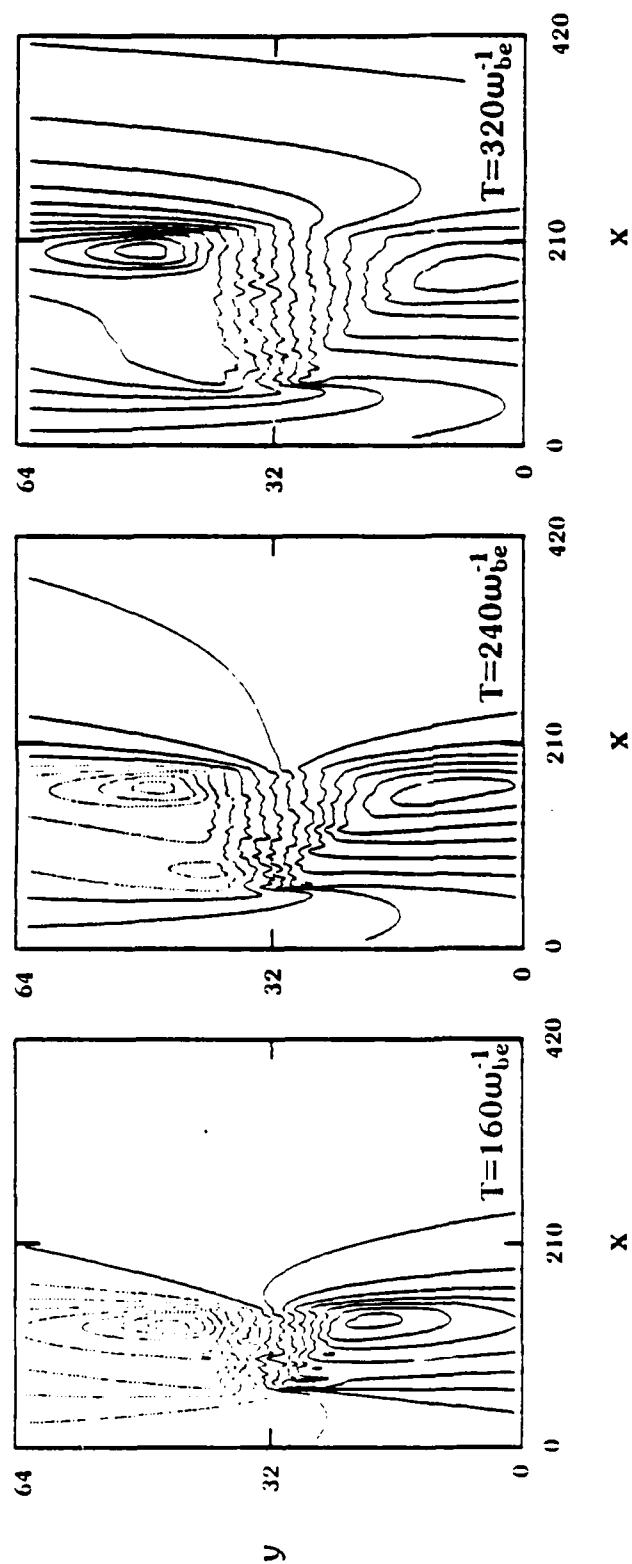


Figure 5. Time-sequence of potential lines for the vacuum propagation case. Potential lines in beam separate as ions are lost from space-charge layer.

The asymmetric ion loss from the beam serves to distort the potential distribution. As these ions gyrate away from the beam the polarization layer is broadened. The polarization electric field then extends over a region much higher than the original beam height at injection.

3.2.2 Beam density and current plots. In addition to distorting the potential distribution, the loss of ions from the space-charge layer allows a net current to flow within the beam. The beam electrons drifting across the magnetic field constitute a current flowing from the head of the beam toward the source. The sense of the resulting $\vec{j} \times \vec{B}$ force is in the correct direction to account for the transverse displacement. This is demonstrated in Figure 6. Here the 10% density contour of the ion component is shown below the net current flow in the beam. The forward half of the beam is discernibly shifted in the \hat{y} direction. Within this portion of the beam a net current in the $-\hat{x}$ direction is evident. Additionally, a current structure flowing from the head to the source persists along the entire length of the positively charged side of the beam.

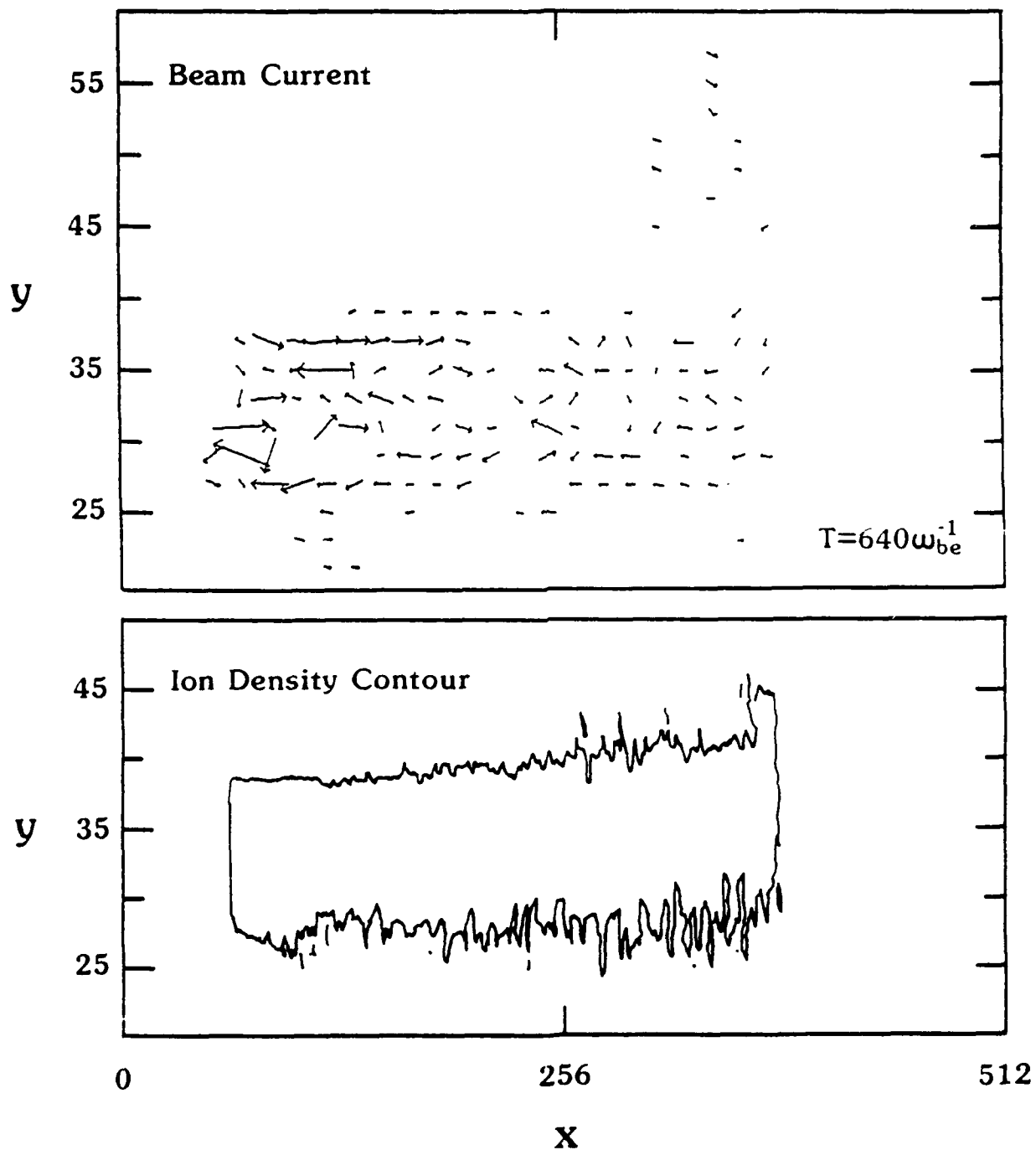


Figure 6. Beam current plot for vacuum case. Ion density contour and current plots are shown separately. Current in right half and lower edge of beam appear to produce $\vec{j} \times \vec{B}$ force to curve beam upward.

4. INJECTION INTO A LOW-DENSITY PLASMA

The presence of an ambient plasma provides a source of particles which responds to the locally induced fields of the beam plasma. The resulting flow of the ambient particles serves to maintain quasi-neutrality in the system. The polarization drift model relies on charge imbalance to drive the beam across the magnetic field. The ambient plasma can partially neutralize the space-charge boundary layers, altering both the trajectory and profile of the beam. Injection as a function of the ratio of ambient to beam plasma density is considered in this section. The cases of $n_p/n_b = 1/100$ and $n_p/n_b = 1/10$ are presented and contrasted with the vacuum injection case.

4.1 Beam Properties as a Function of Relative Density

4.1.1 Beam density and potential contour plots for ambient plasma. Figure 7 depicts the beam contour plots for the case of $n_p/n_b = 1/100$. As in Figure 3 the minimum contour value is 10% of the injection value. During a period of $720\omega_{be}^{-1}$ the beam travels from $x = 60\Delta$ to $x = 420\Delta$. As in the vacuum case, the average propagation velocity is $v_x = 0.5\omega_{be}$, the injection velocity. In this case the beam curvature is visibly more pronounced than the vacuum case. Density estimates along the beam suggest it will degrade to 10% of the injection value after traveling $2.7\rho_i$.

The density contour plots for the $n_p/n_b = 1/10$ case are presented in Figure 8. Here there is a gross distortion of the expected beam trajectory. Close inspection of the two panels shows the beam species to literally separate as the beam initially deflects in the \hat{y} direction. The two streams then recombine and the beam deflects in the opposite direction. However, the head of the beam still has an average velocity in the \hat{x} direction of $v_x = 0.5\omega_{be}^{-1}$. No estimate is made of the distance this beam might travel.

Beam density degradation as a function of ambient plasma density is presented in Figure 9. The density profiles of the beam cross-section are presented in order of increasing ambient density with the vacuum case at the top. In all cases the beam has propagated for a time of $320\omega_{be}^{-1}$ and the cross-section is taken at $x = 161\Delta$. The beam is propagating out of the page in Figure 9. The vertical axis is scaled to the normalized beam density and the horizontal axis is the y axis of the simulation box. The dashed line forming a rectangle

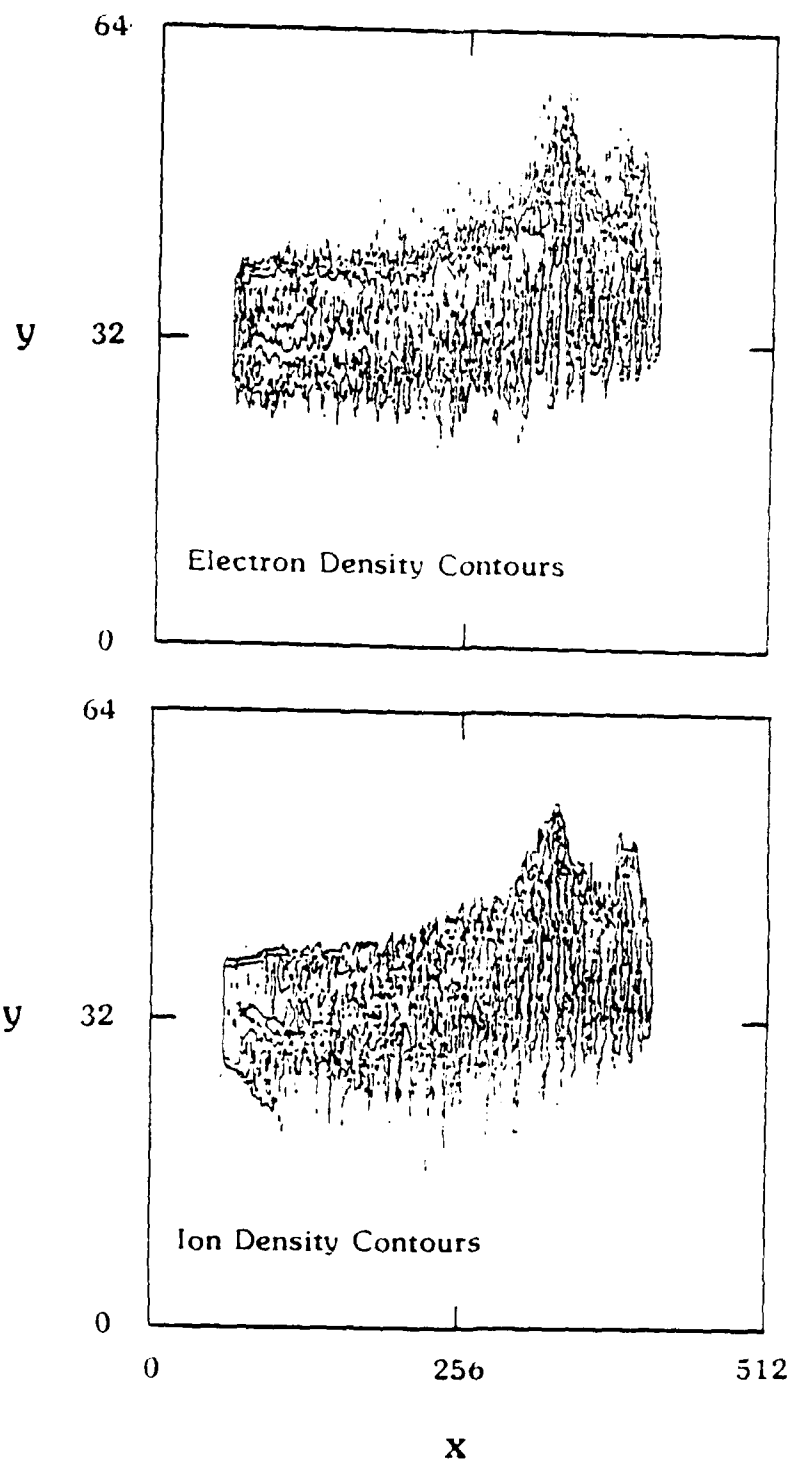


Figure 7. Example of beam propagating in tenuous plasma ($n_p/n_b = 1/100$). Minimum density contour is 10% of injection value. Beam curvature is more pronounced than the vacuum case.

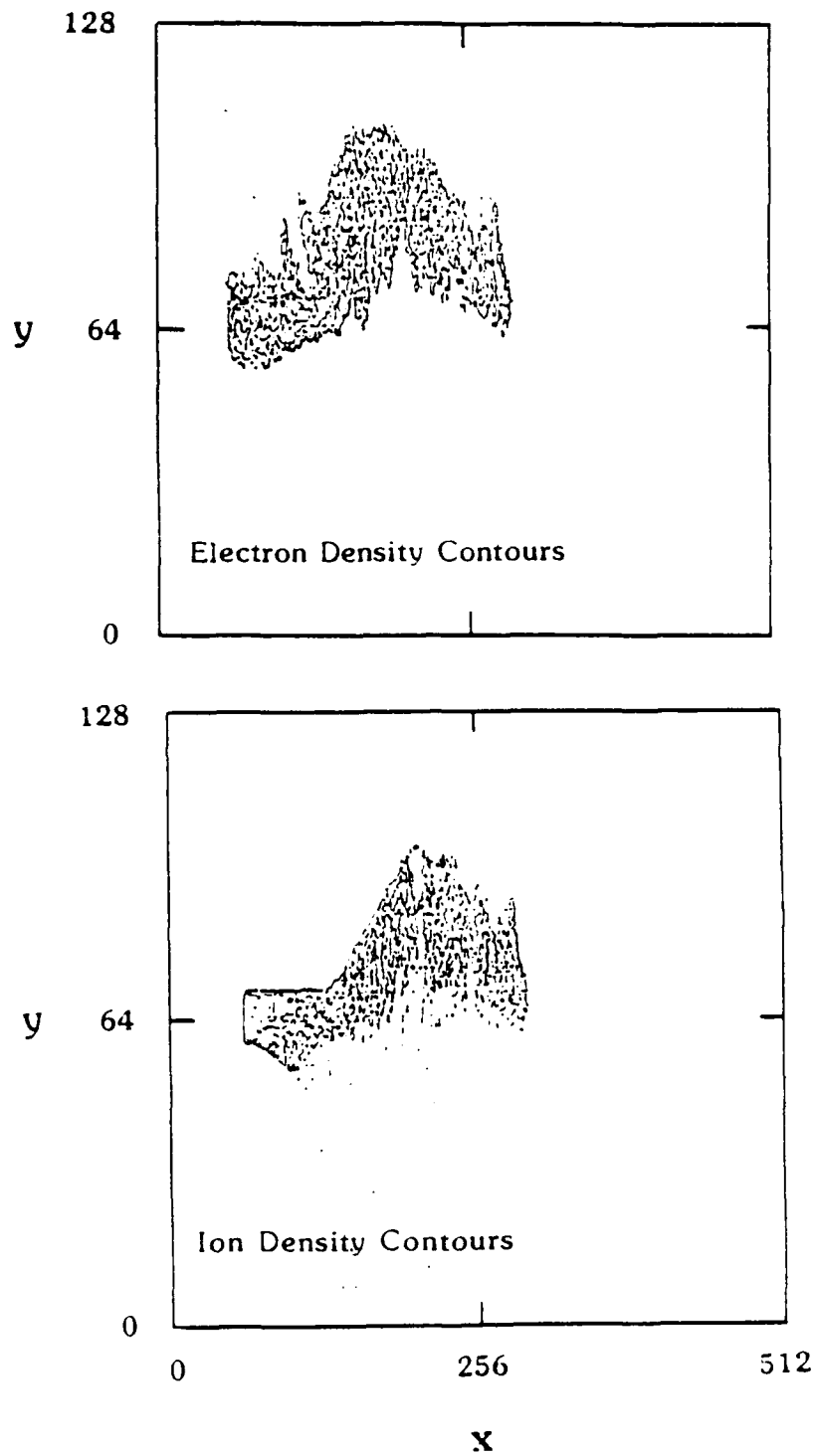


Figure 8. Example of beam propagating in marginally dense plasma
($n_p/n_b = 1/10$). Minimum density contour is 10% of
injection value. Beam curvature is very abrupt.

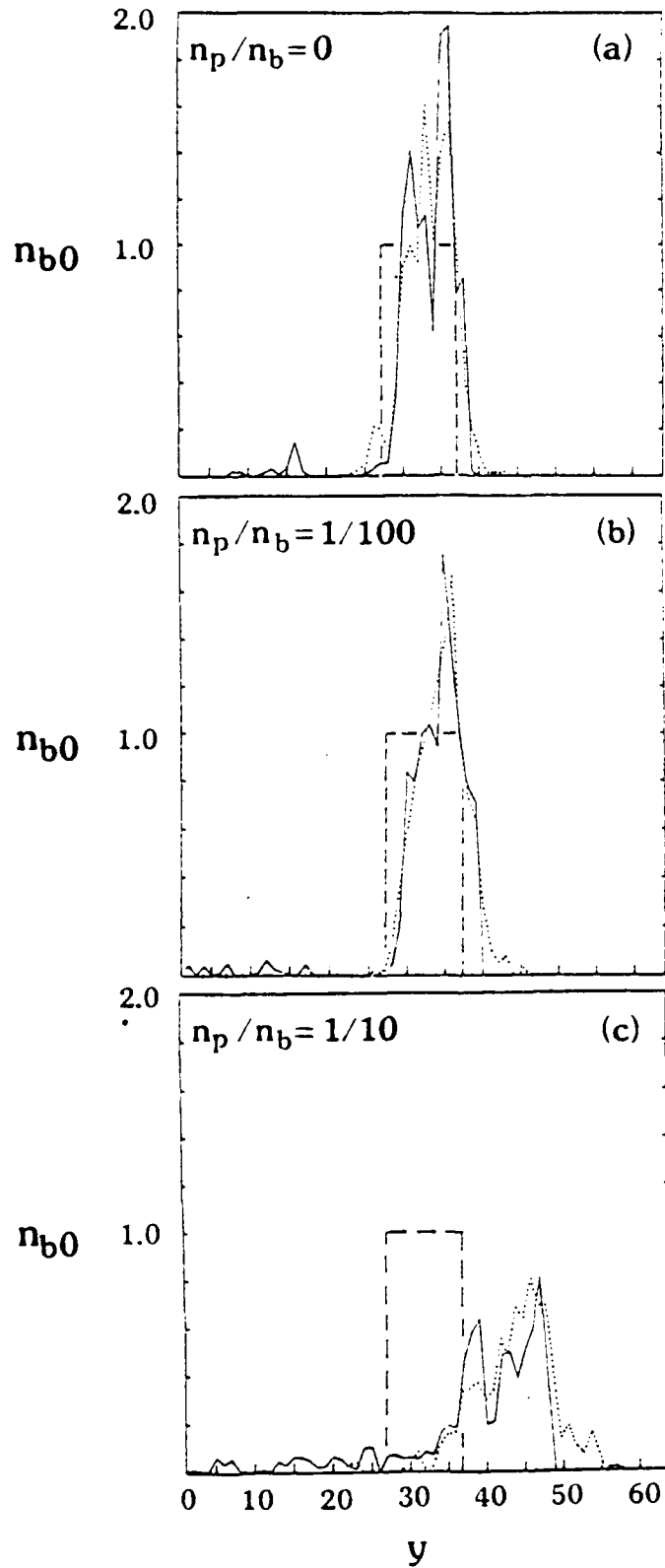


Figure 9. Comparison of density profiles for beams which have propagated for $t = 320 \omega_{be}^{-1}$. Cross-sections are taken at $x = 161\Delta$. (a) Vacuum. (b) Tenuous plasma. (c) Marginally dense plasma.

represents the idealized density profile of the beam cross-section at injection. The solid line represents the density profile of the beam ions. The dotted line represents the density profile of the beam electrons. For the vacuum case shown in panel (a) the beam is slightly offset to the right of the initial injection profile. Ions in noticeable quantities are moving to the left of the positive side of the beam to a distance of approximately 20Δ . For the tenuous plasma case shown in panel (b) the beam is offset to a greater degree than the vacuum case. Also, ions moving to the left of the positive side of the beam extend beyond the boundary of the simulation box. In the case of the marginally dense plasma shown in panel (c) the beam is almost completely outside of the initial injection profile. The ions moving to the left do so in greater quantity than the previous two cases and extend beyond the boundary of the simulation box. In all three cases fluctuations in the ion density are followed closely by electron density fluctuations.

The increase of beam curvature for the cases of interpenetrating ambient plasma is clarified in Figure 10. In this example the 10% density contour is shown below the net beam current for $n_p/n_b = 1/100$. The beam has been propagating for $t = 320 \omega_{be}^{-1}$. A backward flowing current structure has developed along the bottom of the beam. The current is roughly twice the magnitude of the vacuum case shown in Figure 6 and has evolved in half the time. The $\vec{j} \times \vec{B}$ force is therefore larger and can act on the beam for a longer time.

4.1.2 Potential contour plots. Potential distortion as a function of ambient plasma density is presented in Figure 11. The potential plots depicted are companions to those in Figure 9. The vacuum case occupies the left panel. The $n_p/n_b = 1/100$ case in the center panel shows the potential contours have been distended downward in the direction in which ions are being shed from the positive space-charge boundary layer. The contours are tilted slightly upward, coinciding with the beam trajectory. The right panel depicts the $n_p/n_b = 1/10$ case. The potential contours are grossly distorted when compared to the vacuum case. The beam trajectory, however, is still along the contours which indicates an $\vec{E} \times \vec{B}$ drift mechanism.

4.2 Response of the Ambient Plasma. From study of the vacuum case it is obvious that the shedding of ions is partially responsible for the potential

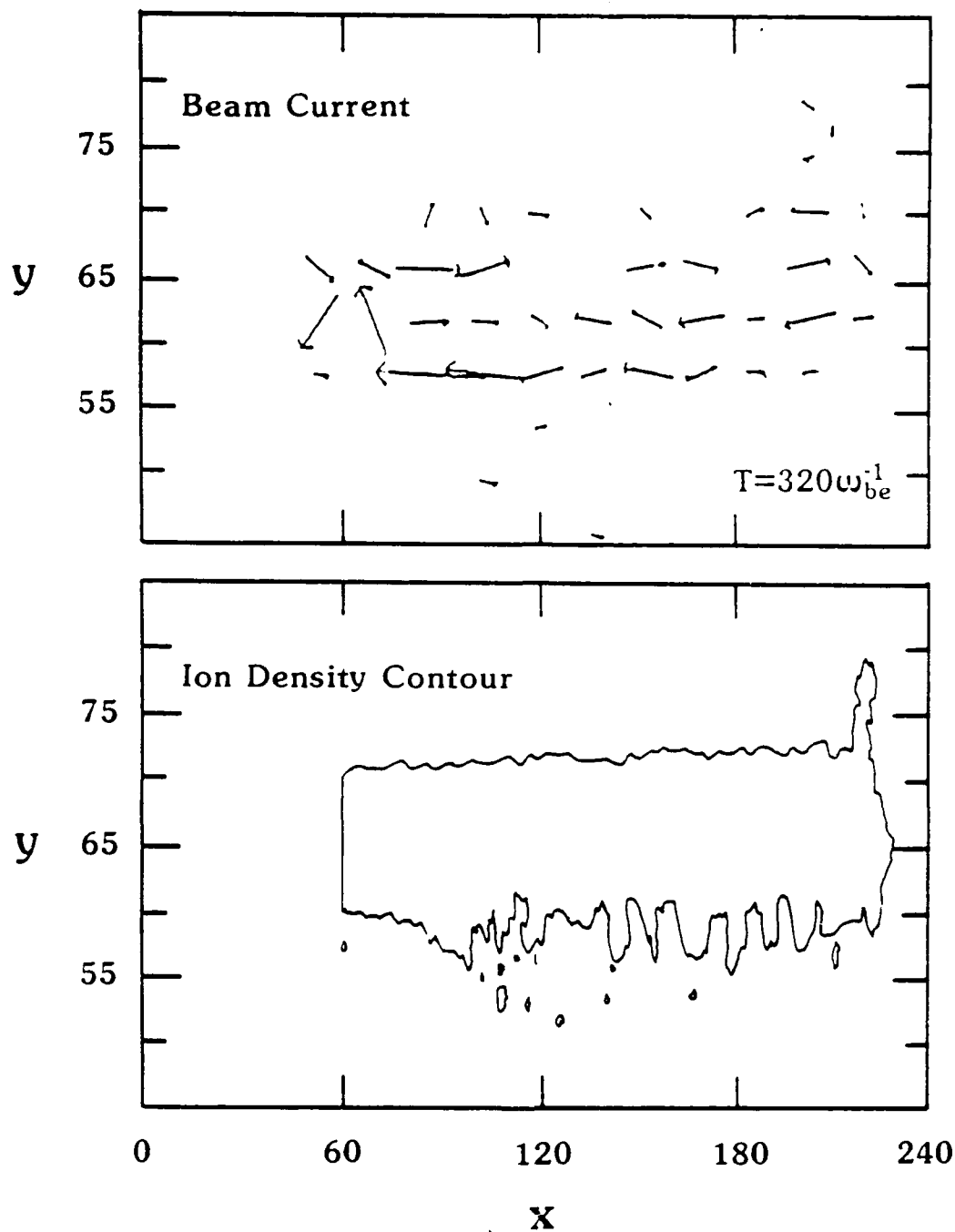


Figure 10. Beam current plot for tenuous plasma case ($n_p/n_b = 1/100$).
Ion density contour and current plots are shown separately.
Current in lower edge appears to produce $\vec{j} \times \vec{B}$ force to
curve beam upward.

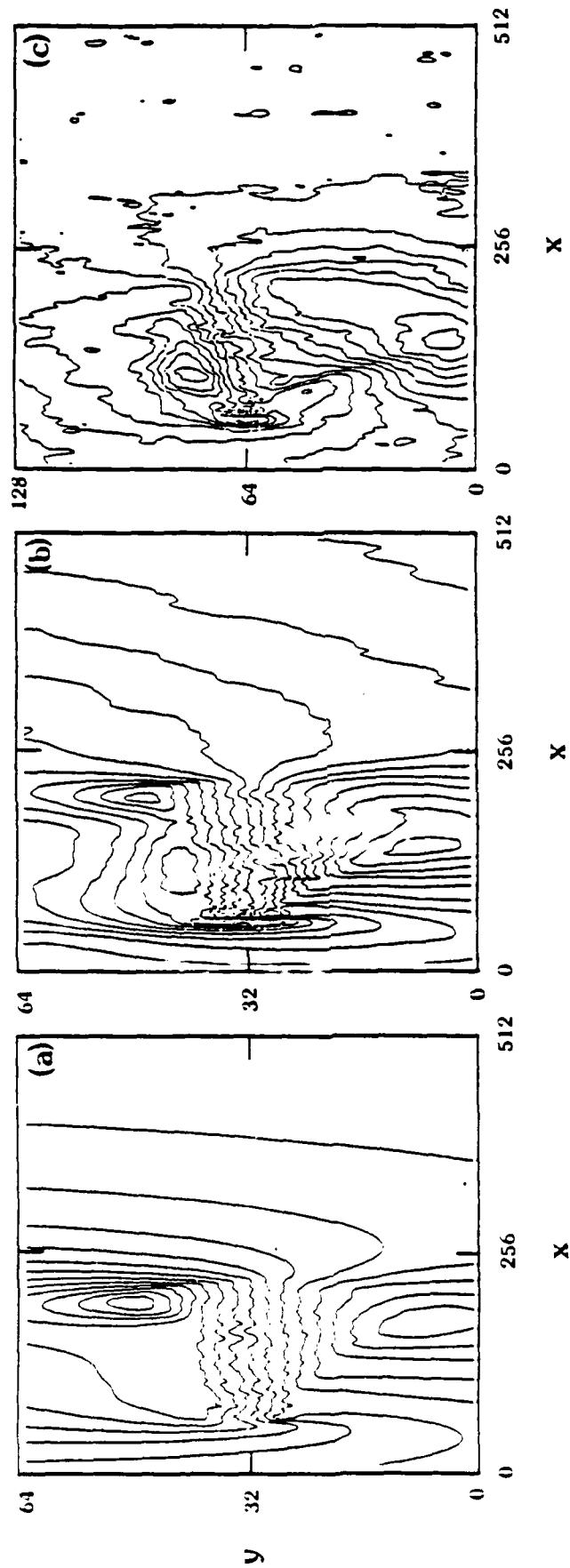


Figure 11. Potential plots of beams which have propagated for $t = 320 \omega_{pe}^{-1}$. (a) Vacuum. (b) Tenuous plasma. (c) Marginally dense plasma.

contour distortion. The presence of ambient plasma enhances this beam ion loss by providing additional shielding of the space-charge layers. This is evident from a consideration of Figure 12. The figure depicts the ambient currents for the $n_p/n_b = 1/100$ case. The current of each species is shown separately. The beam region is identified by the superimposed density contour. Ambient ion currents are shown in the upper panel and ambient electron currents in the lower panel. The obvious difference of the two plots is attributable to magnetization scale lengths. For distances on the order of the beam height the ions are virtually unmagnetized whereas the electrons are strongly magnetized. When acted on by an electric field the ions undergo direct acceleration while the electrons $\vec{E} \times \vec{B}$ drift.

Within the beam region ambient ions are driven by the polarization field. This accounts for the ion current observed flowing across the beam in Figure 12. The ambient ion flow results in the transverse polarization field being reduced. Below the beam the ambient ion current is driven by the field of the beam ions being shed from the positive space-charge layer. The ambient ions are also drawn to the spacecraft since it has become negatively charged.

On the lower side of the beam the ambient electron current is evidence of the polarization region being distended downward. The electrons drifting in the \hat{x} direction imply an electric field in the \hat{y} direction.

The absence of ambient currents in much of the beam region is due to the expulsion of the ambient plasma by the mechanisms described above.

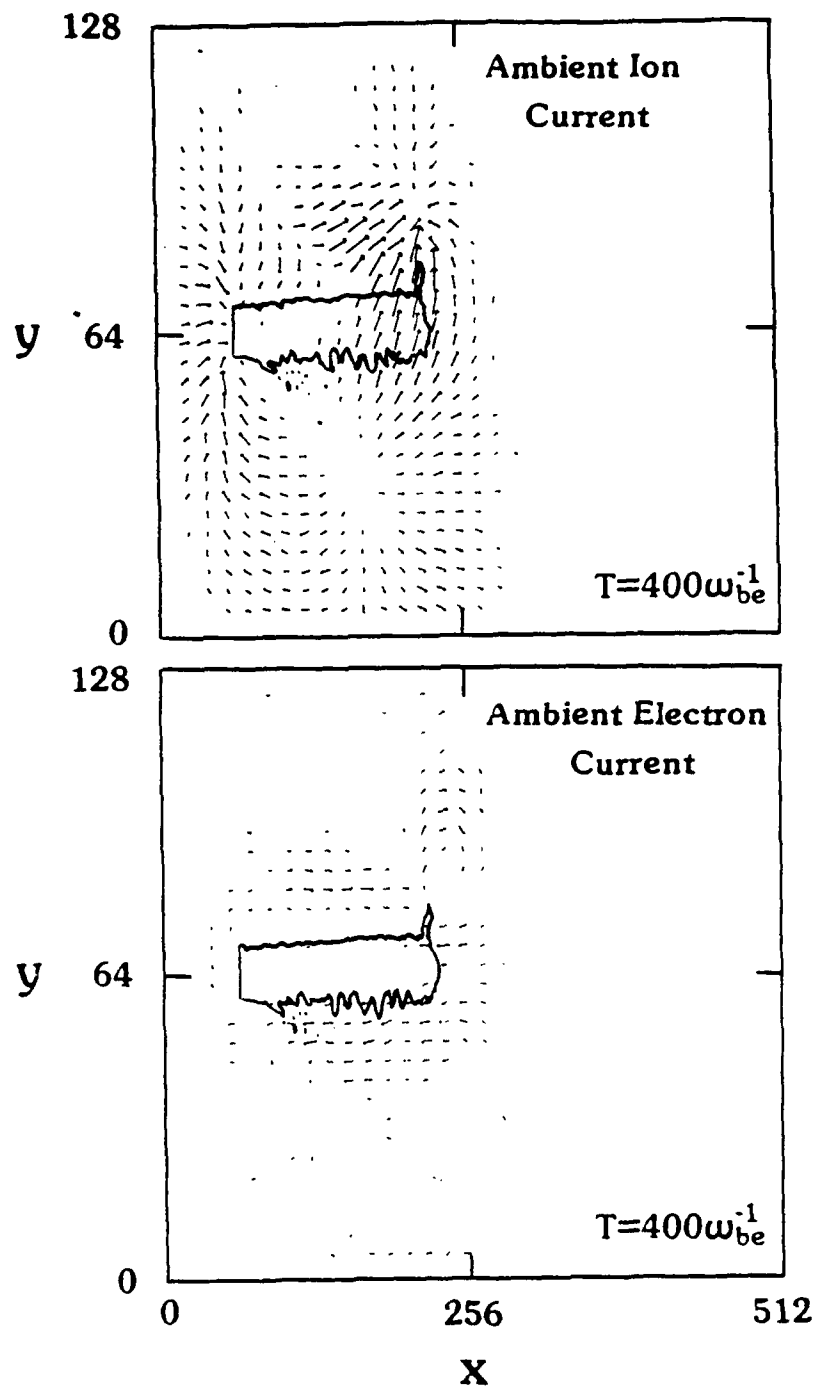


Figure 12. Ambient current plot for tenuous plasma case ($n_p/n_b = 1/100$).
Ion density contour is superimposed. (a) Ambient ion current.
(b) Ambient electron current.

5. SUMMARY AND CONCLUSIONS

In this paper we have investigated the properties of a charge-neutral beam injected into a transverse magnetic field. The beam consisted of ions and electrons. The study made use of two-dimensional electrostatic simulations employing an isolated system model. Motivation for the study stems from an interest in creating long plasma columns in the ionosphere. For a limited range of parameters it is known that a charge-neutral beam can propagate perpendicular to a magnetic field by virtue of collective effects. We have simulated this phenomenon to determine possible limitations on the distance a beam might travel across a magnetic field. It has been shown that when the criteria for the polarization drift model are satisfied, the beam does propagate.

For the case of vacuum injection ($n_p/n_b = 0$) the beam propagates at the injection velocity. The density of the charge-neutral core of the beam is depleted by a combination of beam spreading and particle loss. It is estimated that the beam core will degrade to 10% of its injection density after traveling $4.5\rho_i$. For a 400 eV Argon beam injected across a 0.25 gauss field this is more than 3 kilometers. The beam exhibits a slight curvature in the direction opposite to that of ion gyration in the magnetic field. The large gyroradius of the ions allow some of the outer edge of the beam to be lost from the positive space-charge layer. This leaves a net electron current in the beam flowing toward the source from the head. The resulting $\vec{j} \times \vec{B}$ force is in the correct direction to account for the beam curvature.

In the case of injection into a tenuous plasma ($n_p/n_b = 1/100$) the beam still propagates at the injection velocity. The beam is estimated to degrade to 10% of the injection density after traveling $2.7\rho_i$. Beam curvature is again exhibited and is more pronounced than for the vacuum case. The electron current in the beam is greater than in the vacuum case and is established sooner. The $\vec{j} \times \vec{B}$ force would then be larger, accounting for the increased curving of the beam. The increase in beam electron current is due to the enhanced shielding provided by the ambient plasma. The ambient ions flow directly across the beam, partially shorting the polarization field. This aids the loss of positive charge from the lower space-charge polarization layer. The escaping ions noticeably distend the potential contours and draw the polarization field down from the beam.

Injection into a marginally dense ($n_p/n_b = 1/10$) plasma yields a propagation speed in the \vec{x} direction equal to the injection velocity. No estimate of propagation distance was made for this case. The beam curves drastically and partially separates into distinct streams of ions and electrons. The loss of ions from the beam exceeds that of the tenuous case and the potential contours deviate markedly from those of the other cases.

The presence of the expected polarization field required to drive the beam through a magnetic barrier has been confirmed by our simulations. The beam degradation reported by other investigators⁶ has also been confirmed. The net electron current in the beam and the subsequent beam curvature were unexpected.

Despite the rapid degradation of the beam it appears possible to produce extremely long plasma columns using the transverse injection technique studied in this work. A test of the feasibility of using such a column as an electron collector would require a full three-dimensional simulation.

References

1. D.A. Baker and J.E. Hammel, Demonstration of Classical Plasma Behavior in a Transverse Magnetic Field, Phys. Rev. Lett., 8, 157 (1962).
2. D.A. Baker and J.E. Hammel, Experimental Studies of the Penetration of a Plasma Stream into a Transverse Magnetic Field, Phys. Fluids, 8, 713 (1965).
3. I.I. Demidenko, N.S. Lomino, and V.G. Padalka, Plasma Flow in a Strong Transverse Magnetic Field, Sov. Phys. - Tech. Phys., 16, 1096 (1972).
4. Frank Wessel and Scott Robertson, Polarization of an Intense Space-Charge-Neutral Ion Beam Incident Upon a Magnetic Field, Phys. Fluids, 24, 739 (1981).
5. William Peter and Norman Rostoker, Theory of Plasma Injection into a Magnetic Field, Phys. Fluids, 25, 730 (1982).
6. J.K. Koga, J.L. Geary, T. Tajima and N. Rostoker, Plasma Injection Across Transverse and Curved Magnetic Fields, 1984 Sherwood Theory Conference, April 10-13, Incline Village, Nevada.
7. H. Okuda and S. Hiroe, Diffusion of a Plasma Subject to Neutral Beam Injection, Phys. Fluids, 30, 1160 (1967).
8. Miguel Galvez, Computer Simulations of a Plasma Streaming Across a Magnetic Field, Phys. Fluids, 30, 2729 (1987).
9. Miguel Galvez and Christopher Barnes, Two-Dimensional Electrostatic Simulations of Plasma Propagation Perpendicular to a Magnetic Field, submitted to Phys. Fluids (1987).
10. E. Ott and W.M. Manheimer, Cross-Field Injection, Propagation, and Energy Deposition of Intense Ion Beams with Application to Tokamak Plasma Heating, Nucl. Fusion, 17, 1057 (1977).

11. T. Ohkawa, New Methods of Driving Plasma Current in Fusion Devices, Nucl. Fusion, 10, 185 (1970).
12. G. Haerendel and R.Z. Sagdeev, Artificial Plasma Jet in the Ionosphere, Adv. Space Res., 1, 29 (1981).
13. P.M. Kintner and M.C. Kelly, ion Beam Produced Plasma Waves Observed by the $\delta n/n$ Plasma Receiver During the Porcupine Experiment, Adv. Space Res., 1, 107 (1981).
14. I. Roth, C.W. Carlson, M.K. Hudson, R.L. Lysak, Simulations of Beam Excited Minor Species Gyroharmonics in the Porcupine Experiment, J. Geophys. Res., 88, 8115 (1983).
15. R. Pottelette, J.M. Illiano, O.H. Bauer and R. Treumann, Observation of High-Frequency Turbulence Induced by an Artificial Ion Beam in the Ionosphere, J. Geophys. Res., 89, 2324 (1984).
16. R. Pottelette, R. Treumann, O.H. Bauer and J.P. Lebreton, Generation of Electrostatic Shocks and Turbulence Through the Interactions of Conics with the Background Plasma, Geophys. Res. Lett., 12, 57 (1985).
17. M. Malingre and R. Pottelette, Excitation of Broadband Electrostatic Noise and of Hydrogen Cyclotron Waves by a Perpendicular Ion Beam in a Multi-Ion Plasma, Geophys. Res. Lett., 12, 275 (1985).
18. S. Chapman and V.C.A. Ferraro, A New Theory of Magnetic Storms, Terr. Mag., 36, 77 (1931).
19. James L. Tuck, Plasma Jet Piercing of Magnetic Fields and Entropy Trapping into a Conservative System, Phys. Rev. Lett., 3, 313 (1959).
20. D.J. Rose and M. Clark, Jr., Plasma and Controlled Fusion, (The M.I.T. Press, Massachusetts Institute of Technology, and John Wiley and Sons, Inc., New York, 1961) p. 416.

21. S. Chapman, The Motion of a Neutral Ionized Stream in the Earth's Magnetic Field, Proc. Cambridge Phil. Soc., 21, 577 (1923).
22. G. Schmidt, Plasma Motion Across Magnetic Fields, Phys. Fluids, 3, 961 (1960).
23. Lennart Lindberg, Plasma Flow in a Curved Magnetic Field, Astrophys. Space Sci., 55, 203 (1978).
24. P.L. Pritchett and R.M. Winglee, The Plasma Environment During Particle Beam Injection Into Space Plasmas 1. Electron Beams, J. Geophys. Res., 92, 7673 (1987).
25. R.M. Winglee and P.L. Pritchett, The Plasma Environment During Particle Beam Injection Into Space Plasmas 2. Charge-Neutral Beams, J. Geophys. Res., 92, 7689 (1987).



MISSION of Rome Air Development Center

RADC plans and executes research, development, test and selected acquisition programs in support of Command, Control, Communications and Intelligence (C³I) activities. Technical and engineering support within areas of competence is provided to ESD Program Offices (POs) and other ESD elements to perform effective acquisition of C³I systems. The areas of technical competence include communications, command and control, battle management information processing, surveillance sensors, intelligence data collection and handling, solid state sciences, electromagnetics, and propagation, and electronic reliability/maintainability and compatibility.